Ocean Systems Engineering, *Vol. 6, No. 4 (2016) 377-400*
DOI: http://dx.doi.org/10.12989/ose.2016.6.4.377

Risk free zone study for cylindrical objects dropped into the water

Gong Xiang[1], Lothar Birk[1], Linxiong Li[2], Xiaochuan Yu[*1] and Yong Luo[3]

[1]*School of Naval Architecture and Marine Engineering, University of New Orleans, New Orleans, LA, USA*
[2]*Department of Mathematics, University of New Orleans, New Orleans, LA, USA*
[3]*School of Naval Architecture, Ocean and Civil Engineering, Shanghai Jiao Tong University, Shanghai, China*

(Received August 18, 2016, Revised November 3, 2016, Accepted November 7, 2016)

Abstract. Dropped objects are among the top ten causes of fatalities and serious injuries in the oil and gas industry (DORIS, 2016). Objects may accidentally fall down from platforms or vessels during lifting or any other offshore operation. Proper planning of lifting operations requires the knowledge of the risk-free zone on the sea bed to protect underwater structures and equipment. To this end a three-dimensional (3D) theory of dynamic motion of dropped cylindrical object is expanded to also consider ocean currents. The expanded theory is integrated into the authors' Dropped Objects Simulator (DROBS). DROBS is utilized to simulate the trajectories of dropped cylinders falling through uniform currents originating from different directions (incoming angle at 0^o, 90^o, 180^o, and 270^o). It is found that trajectories and landing points of dropped cylinders are greatly influenced by the direction of current. The initial conditions after the cylinders have fallen into the water are treated as random variables. It is assumed that the corresponding parameters orientation angle, translational velocity, and rotational velocity follow normal distributions. The paper presents results of DROBS simulations for the case of a dropped cylinder with initial drop angle at 60^o through air-water columns without current. Then the Monte Carlo simulations are used for predicting the landing point distributions of dropped cylinders with varying drop angles under current. The resulting landing point distribution plots may be used to identify risk free zones for offshore lifting operations.

Keywords: dropped cylindrical object; landing point distribution; Monte Carlo simulation; risk free zone; current

1. Introduction

Dropped objects are one of the principal causes of accidents in the oil and gas industry. The frequency of dropping tools and equipment into the sea during lifting operations or other offshore operations is significant. DNV (1996) reports data recorded by the UK Department of Energy for the period 1980-1986:

- Over the 7 year period 825 crane years were recorded with an estimated total of 3.7 million lifting operations. This corresponds to 4500 lifts to and from vessels per crane per year.
- 81 incidents of dropped objects occurred during the reporting period which is equivalent to a frequency of $2.2 \cdot 10^{-5}$ per lift. The drop frequency has actually been slightly higher with

*Corresponding author, Professor, E-mail: xyu5@uno.edu

Copyright © 2016 Techno-Press, Ltd.
http://www.techno-press.org/?journal=ose&subpage=7 ISSN: 2093-6702 (Print), 2093-677X (Online)

$3.0 \cdot 10^{-5}$ per lift for lifts above 20 tons.

- Of the dropped objects 70% fell on deck and 30% fell into the sea.

In the risk assessment for pipelines (DNV, 2010), the object excursions on the seabed are assumed to follow a normal distribution. However, according to ABS (2013) specialized techniques are still required to predict the trajectory of dropped objects and the subsequent likelihood of striking additional structure and equipment as well as predicting the consequences of such impacts. Therefore, trajectory dynamics of objects falling into the water, their landing points, and the layout of a risk-free zone on the seabed are of interest for the protection of subsea oil and gas production installations.

Luo and Davis (1992) simulated the 2D motion of falling objects by solving the differential equations of motion. Illustrative parametric studies are carried out by using a computer program called DELTA. It was found that the horizontal motion and velocity of dropped objects are greatly affected by the drop angle and drop height. Also, horizontal excursion at the seabed level is found to be significantly influenced by drop angle and current. However, waves seem to have limited effects on both horizontal excursion and maximum velocity. Colwill and Ahilan (1992) performed multiple numerical studies of trajectories of two dropped drill casings by using the same computer program, DELTA. These studies confirmed that drop height above waterline and the initial drop angle are key parameters influencing the horizontal velocity. Reliability-based impact analysis successfully established the relation between impact velocity and the probability of its exceedance.

Chu, Gilles *et al.* (2005), Chu and Fan (2006) developed a 3D motion program, IMPACT35, to simulate objects falling through a single fluid (e.g., air, water, or sediment) and through the interface of different fluids (air-water and water-sediment interface). Drag, lift force, and moments were linearized with temporally varying coefficients in the time domain. Chu, Gilles *et al*. (2005) report the trajectories of falling cylinders obtained from model tests. Longitudinal center of gravity (LCG), initial velocity, and drop angle were varied. IMPACT35 has been validated by comparing its results with the experimental data. As expected, LCG, initial velocity, and drop angle are found to be critical factors influencing the underwater trajectories of dropped objects.

Xiang, Birk *et al*. (2016a) proposed a new 3D theory which also considers the effect of axial rotation on dropped cylindrical objects with uniform mass distribution. It is based on amodification of maneuvering equations from slender rigid body theory. A numerical tool called Dropped Objects Simulator (DROBS) has been successfully developed based on this 3D theory to investigate various factors that may affect the trajectories, including drop angle, normal drag coefficient, binormal drag coefficient, and rolling frequency. The simulated trajectories agree well with data from model tests (Aanesland 1987). Plots of landing points for small rolling frequency cases are obtained from numerical simulations by varying the initial drop angle from 0^{o} to 90^{o}. Xiang, Birk *et al*. (2016b) further extended the 3D theory (Xiang, Birk *et al*. 2016a) to study the dynamic motion of dropped cylindrical objects with nonuniform mass distributions. Simulations revealed that the LCG position affects the trajectories and landing points of dropped cylindrical objects. The calculated trajectories match the experimental published in Chu, Gilles *et al*. (2005) very well.

Yasseri (2014) experimentally investigated the falling of model-scale cylinders through calm water with low initial entry velocity and concluded that the landing point locations of free-falling cylinders are within 10% of the water depth with 50% of probability, within 20% of the water depth with 80% of probability, within 30% of the water depth with 90% of probability, within 40% of the water depth with 95% of probability, and within 50% of the water depth with 98% of probability.

Awotahegn (2015) performed a series of model tests to investigate the trajectories and excursions at the seabed of two drill pipes (8'' and 12'') falling from defined heights above the water surface into calm water. He plotted and statistically analyzed the distribution of landing points on the seabed for drop angles from 0^o to 90^o. After comparing them with the results from a simplified method by DNV (2010), Awotahegn (2015) concluded that the assessment procedure recommended by DNV (2010) is generally conservative.

Majed (2013) presented nonlinear dynamic simulations of dropped objects for an assessment of dropped object trajectories by incorporating detailed 3D hydrodynamic models of complex object geometries. In addition, the entire impact zone is determined using Monte-Carlo simulations. The object's initial drop angle after being fully immersed is used as a random variable.

In this paper the 3D theory reported in Xiang (2016b) is extended to consider the underwater dynamic motion of a dropped cylindrical object under the influence of currents from different directions. The updated Dropped Objects Simulator (DROBS) is utilized to investigate how uniform currents from different directions (incoming angle at 0^o, 90^o, 180^o, and 270^o) affect the trajectories of dropped cylinders. It is found that the trajectory and landing point of dropped cylinders are greatly influenced by currents. During the simulations initial conditions after water entry of the dropped cylinder are treated as random variables. Values for drop angle, translational velocity, and rotational velocity are assumed to follow normal distributions. Firstly, the landing point distribution is obtained through a Monte Carlo simulation of the trajectories without currents and a fixed initial drop angle of 60^o. lso, Secondly, Monte Carlo simulations are used for predicting the landing point distribution of dropped cylinders under current with drop angles varying from 0^o to 90^o. Plots of landing point distributions , probability density function (PDF), and cumulative distribution function (CDF) have been given to provide a simple way to estimate risk-free zones.

2. 3D theory for dropped objects

In Fig. 1, ***OXYZ*** is the global coordinate system, where X-Y represents the still-water surface and Z-axis points vertical upwards. The second coordinate system ***oxyz*** is a local coordinate system fixed to the cylinder. The x-axis is identical to the cylinder axis, the y-axis points in binormal direction, and the z-axis points in normal direction. The origin ***o*** is located at the geometric center.

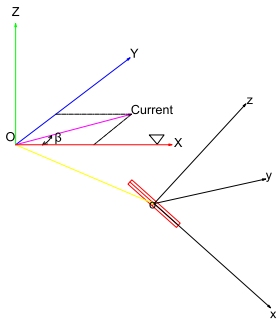

Fig. 1 Coordinate systems for equations of motion in three dimensions

A 3D theory for the motions of dropped cylinders with nonuniform mass distribution is captured by the following set of equations (Aanesland 1987, Xiang, Birk *et al*. 2016b)

$$(m-\rho\nabla)g\sin(\theta)+F_{dx}=m\left(\dot{U}_1+U_3\Omega_2-U_2\Omega_3-X_G{\Omega_2}^2-X_G{\Omega_3}^2\right) \tag{1}$$

$$\begin{aligned}-(m-\rho\nabla)g\cos(\theta)\sin(\phi)+F_{Ly}+F_{dy}=&\left\{m_{22}\dot{U}_2+U_1m_{t2}U_2-U_1(x_tm_{t2})\Omega_3\right\}\\&+m\left(\dot{U}_2+U_1\Omega_3-U_3\Omega_1+X_G\Omega_1\Omega_2+X_G\dot{\Omega}_3\right)\end{aligned} \tag{2}$$

$$\begin{aligned}-(m-\rho\nabla)g\cos(\theta)\cos(\phi)+F_{Lz}+F_{dz}=&\left\{m_{33}\dot{U}_3+U_1m_{t3}U_3-U_1(x_tm_{t3})\Omega_2\right\}\\&+m\left(\dot{U}_3+U_2\Omega_1-U_1\Omega_2+X_G\Omega_1\Omega_3-X_G\dot{\Omega}_2\right)\end{aligned} \tag{3}$$

$$\dot{\Omega}_1=c \tag{4}$$

$$\begin{aligned}M_{by}+M_{Ly}+M_{dy}=&\left\{-U_1(m_{33}+x_tm_{t3})U_3+U_1{x_t}^2m_{t3}\Omega_2+m_{55}\dot{\Omega}_2\right\}\\&+M_{55}\dot{\Omega}_2+(M_{44}-M_{66})\Omega_1\Omega_3-mX_G(\dot{U}_3-U_1\Omega_2+U_2\Omega_1)\end{aligned} \tag{5}$$

$$\begin{aligned}M_{bz}+M_{Lz}+M_{dz}=&\left\{-U_1(m_{22}+x_tm_{t2})U_2+U_1{x_t}^2m_{t2}\Omega_3+m_{66}\dot{\Omega}_3\right\}\\&+M_{66}\dot{\Omega}_3+(M_{55}-M_{44})\Omega_1\Omega_2+mX_G(\dot{U}_2+U_1\Omega_3-U_3\Omega_1)\end{aligned} \tag{6}$$

The following parameters are used:

c rolling frequency decaying rate
D diameter of the cylinder
g acceleration of gravity
L length of the cylinder
m mass of cylinder
m_{22} added mass in sway direction from strip theory
m_{33} added mass in heave direction from strip theory
m_{55} added mass in pitch direction from strip theory
m_{66} added mass in yaw direction from strip theory
m_{t2} 2D added mass coefficient in sway direction at the trailing edge
m_{t3} 2D added mass coefficient in heave direction at the trailing edge
M_{44} moment of inertia in roll direction
M_{55} moment of inertia in pitch direction
M_{66} moment of inertia in yaw direction
x_t longitudinal position of effective trailing edge
X_G longitudinal center of gravity (LCG)
∇ volume of cylinder
U_1 translational velocity in x direction
U_2 translational velocity in y direction
U_3 translational velocity in z direction
Ω_1 rotational velocity in x direction (rolling frequency)
Ω_2 rotational velocity in y direction (pitching frequency)
Ω_3 rotational velocity in z direction (yawing frequency)
ϕ instantaneous Euler angle around X-axis
θ instantaneous Euler angle around Y-axis

ψ instantaneous Euler angle around Z-axis
ν kinematic viscosity of water
ρ density of water

Translational and rotational motions in x-, y- and z-directions are obtained at each time step during simulations. The global Euler angles ϕ, θ, and ψ are obtained from the local rotational velocity components Ω_1, Ω_2, and Ω_3 through the transformation in Eqs. (7)-(9).

$$\dot{\phi} = \Omega_1 + \frac{\Omega_2 \sin(\phi) + \Omega_3 \cos(\phi)}{\cos(\theta)} \sin(\theta) \tag{7}$$

$$\dot{\theta} = \Omega_2 \cos(\phi) - \Omega_3 \sin(\phi) \tag{8}$$

$$\dot{\Psi} = \frac{\Omega_2 \sin(\phi) + \Omega_3 \cos(\phi)}{\cos(\theta)} \tag{9}$$

M_{by} and M_{bz} are the moments with respect to y- and z-axis caused by the off-center weight

$$M_{by} = X_G mg \cos(\theta) \cos(\phi) \tag{10}$$

$$M_{bz} = -X_G mg \cos(\theta) \sin(\phi) \tag{11}$$

Slender body theory assumes that geometries vary smoothly. The cutoff ends of the cylinders do not satisfy this condition. Effects of the trailing edge of the cylinder are captured with an additional force component according to Newman (1977). The trailing edge force components are marked by curly brackets in Eqs. (2), (3), (5), and (6). The longitudinal position of the effective trailing edge is represented by the parameter x_t. The required 2D added masses, a_{22} and a_{33}, are calculated as follows (Newman 1977)

$$a_{22}(x) = a_{33}(x) = \pi \left(\frac{D}{2}\right)^2 \rho, \qquad -0.5L < x < 0.5L \tag{12}$$

Then, 2D added mass effects of the trailing edge in sway and heave direction are

$$m_{t2} = a_{22}(x = x_t) \tag{13}$$

$$m_{t3} = a_{33}(x = x_t) \tag{14}$$

Added masses and forces for the plane normal to the cylinder axis are derived using a strip-theory approach

$$m_{22} = \int_L a_{22}(x)\, \mathrm{d}x \tag{15}$$

$$m_{33} = \int_L a_{33}(x)\, \mathrm{d}x \tag{16}$$

$$m_{55} = \int_L a_{33}(x) x^2\, \mathrm{d}x \tag{17}$$

$$m_{66} = \int_L a_{22}(x) x^2\, \mathrm{d}x \tag{18}$$

Drag forces F_{dx}, F_{dy}, and F_{dz} acting in x-, y- and z-direction respectively, are obtained by a Morison type equation. M_{dy} and M_{dz} are the corresponding drag moments

$$F_{dx} = \begin{cases} -0.664\pi \mathrm{D}\sqrt{\nu\rho^2 L}U_1\sqrt{|U_1|} - \frac{1}{8}\rho\pi C_{dx}D^2U_1|U_1|, & \text{for laminar flow} \\ -(\frac{0.455}{(\log Re)^{2.58}} - \frac{A}{Re})\frac{1}{2}\rho\pi \mathrm{D}L{U_1}^2 - \frac{1}{8}\rho\pi C_{dx}D^2U_1|U_1|, & \text{for transition} \\ -\frac{0.455}{(\log Re)^{2.58}}\frac{1}{2}\rho\pi \mathrm{D}L{U_1}^2 - \frac{1}{8}\rho\pi C_{dx}D^2U_1|U_1|, & \text{for turbulent flow} \end{cases} \tag{19}$$

$$F_{dy} = 0.5\int_{-0.5L}^{0.5L}\rho C_{dy}DU_y(x)\left|U_y(x)\right|\mathrm{d}x \tag{20}$$

$$F_{dz} = 0.5\int_{-0.5L}^{0.5L}\rho C_{dz}DU_z(x)|U_z(x)|\,\mathrm{d}x \tag{21}$$

$$M_{dy} = -0.5\int_{-0.5L}^{0.5L}\rho C_{dz}DxU_z(x)|U_z(x)|\,\mathrm{d}x \tag{22}$$

$$M_{dz} = 0.5\int_{-0.5L}^{0.5L}\rho C_{dy}DxU_y(x)\left|U_y(x)\right|\mathrm{d}x \tag{23}$$

The first term in the longitudinal force Eq. (19) represents a skin friction force which uses a drag coefficient according to (Schlichting 1979) and the second term represents a form drag component. The longitudinal drag coefficient C_{dx} follows from Fig. 21, Chapter 3, pg. 12 in Hoerner (1958). The transverse drag coefficients C_{dy} and C_{dz} are calculated based on empirical formula by Rouse (1938)

$$C_{dy}\ or\ C_{dz} = \begin{cases} 1.9276 + \frac{8}{Re}, & Re \le 12 \\ 1.261 + \frac{16}{Re}, & 12 < Re \le 180 \\ 0.855 + \frac{89}{Re}, & 180 < Re \le 2000 \\ 0.84 + 0.00003Re, & 2000 < Re \le 12000 \\ 1.2 - \frac{4}{\delta}, & 12000 < Re \le 150000,\ \delta \ge 10 \\ 0.835 - \frac{0.35}{\delta}, & 12000 < Re \le 150000,\ 2 \le \delta < 10 \\ 0.7 - \frac{0.08}{\delta}, & 12000 < Re \le 150000,\ \delta < 2 \\ 1.875 - 0.0000045Re, & 150000 < Re \le 350000 \\ \frac{1}{\frac{641550}{Re}+1.5}, & Re > 350000 \end{cases} \tag{24}$$

$\delta = L/D$ is the cylinder's aspect ratio. The Reynolds numbers are position dependent and are formed with the local transverse relative velocities (see Eqs. (32) and (33)) corresponding to the direction of the drag coefficient: $Re = \frac{U_y(x)D}{\nu}$ for C_{dy}; $Re = \frac{U_z(x)D}{\nu}$ for C_{dz}.

As shown in Fig. 1, currents have the speed $V_{current}$ and flow in direction β measured with respect to the global positive X-axis. The velocity components V_{cX}, V_{cY}, and V_{cZ} of the current in global X-, Y- and Z-directions are

$$V_{cX} = V_{current}\cos(\beta) \tag{25}$$

$$V_{cY} = V_{current}\sin(\beta) \tag{26}$$

$$V_{cZ} = 0 \tag{27}$$

After transformation from global coordinates (***OXYZ***) into local coordinates (***oxyz***) (John and

Francis 1962), the velocity components of the current in x-, y- and z-direction, V_{cx}, V_{cy}, and V_{cz} can be expressed as

$$\begin{aligned} V_{cx} &= V_{cX}\cos(\theta)\cos(\psi) + V_{cY}\cos(\theta)\sin(\psi) \\ V_{cy} &= V_{cX}\{-\cos(\phi)\sin(\psi) + \sin(\phi)\sin(\theta)\cos(\psi)\} \\ &\quad + V_{cY}\{\cos(\phi)\cos(\psi) + \sin(\phi)\sin(\theta)\sin(\psi)\} \end{aligned} \tag{29}$$

$$\begin{aligned} V_{cz} &= V_{cX}\{\sin(\phi)\sin(\psi) + \cos(\phi)\sin(\theta)\cos(\psi)\} \\ &\quad + V_{cY}\{-\sin(\phi)\cos(\psi) + \cos(\phi)\sin(\theta)\sin(\psi)\} \end{aligned} \tag{30}$$

The local relative velocities, U_x, $U_y(x)$ and $U_z(x)$ between water and cylinder are given as

$$U_x = V_{cx} - U_1 \tag{31}$$

$$U_y(x) = V_{cy} - (U_2 + \Omega_3 x), \qquad -0.5L < x < 0.5L \tag{32}$$

$$U_z(x) = V_{cz} - (U_3 - \Omega_2 x), \qquad -0.5L < x < 0.5L \tag{33}$$

Lift forces and moments are also considered in Eqs. (1) through (6). Lift forces and moments are caused by the axial rolling motion and estimated applying Kutta-Joukowski's lift theorem (1941) for a cylinder in ideal flow (potential theory). F_{Ly} and F_{Lz} are lift forces in local y- and z-direction, and M_{Ly} and M_{Lz} are the corresponding moments with respect to y- and z- axis. Γ is the circulation around the cylinder axis

$$F_{Ly} = \int_{-0.5L}^{0.5L} \rho U_z(x)\Gamma \,\mathrm{d}x = \int_{-0.5L}^{0.5L} \rho U_z(x)\pi D\Omega_1 \frac{D}{2}\,\mathrm{d}x \tag{34}$$

$$F_{Lz} = -\int_{-0.5L}^{0.5L} \rho U_y(x)\Gamma \,\mathrm{d}x = -\int_{-0.5L}^{0.5L} \rho U_y(x)\pi D\Omega_1 \frac{D}{2}\,\mathrm{d}x \tag{35}$$

$$M_{Ly} = \int_{-0.5L}^{0.5L} \rho U_y(x)\Gamma\, x \,\mathrm{d}x = \int_{-0.5L}^{0.5L} \rho U_y(x)\pi D\Omega_1 \frac{D}{2} x \,\mathrm{d}x \tag{36}$$

$$M_{Lz} = \int_{-0.5L}^{0.5L} \rho U_z(x)\Gamma\, x \,\mathrm{d}x = \int_{-0.5L}^{0.5L} \rho U_z(x)\pi D\Omega_1 \frac{D}{2} x \,\mathrm{d}x \tag{37}$$

After solving translational velocity components U_1, U_2, and U_3 at each time step by a Runge-Kutta 4th order method (Nagle, Saff *et al*. 2008), the transformation from local coordinate system to global system is realized by Eqs. (38)-(40) (John and Francis 1962)

$$\begin{aligned} \dot{X} &= U_1\cos(\theta)\cos(\psi) + U_2\{-\cos(\phi)\sin(\psi) + \sin(\phi)\sin(\theta)\cos(\psi)\} \\ &\quad + U_3\{\sin(\phi)\sin(\psi) + \cos(\phi)\sin(\theta)\cos(\psi)\} \end{aligned} \tag{38}$$

$$\begin{aligned} \dot{Y} &= U_1\cos(\theta)\sin(\psi) + U_2\{\cos(\phi)\cos(\Psi) + \sin(\phi)\sin(\theta)\sin(\psi)\} \\ &\quad + U_3\{-\sin(\phi)\cos(\psi) + \cos(\phi)\sin(\theta)\sin(\psi)\} \end{aligned} \tag{39}$$

$$\dot{Z} = -U_1\sin(\theta) + U_2\big(-\sin(\phi)\cos(\theta)\big) + U_3\cos(\phi)\cos(\theta) \tag{40}$$

3. Numerical study of dropped objects

3.1 Dropped object: Cylinder #1 with no current

Table 1 Properties of the cylinder #1

Parameters	**Unit**	**Value**
Model scale	-	1:15
Length	m	0.152
Mass per length	kg/m	2.120
Diameter	m	0.040
LCG	m	0.0074

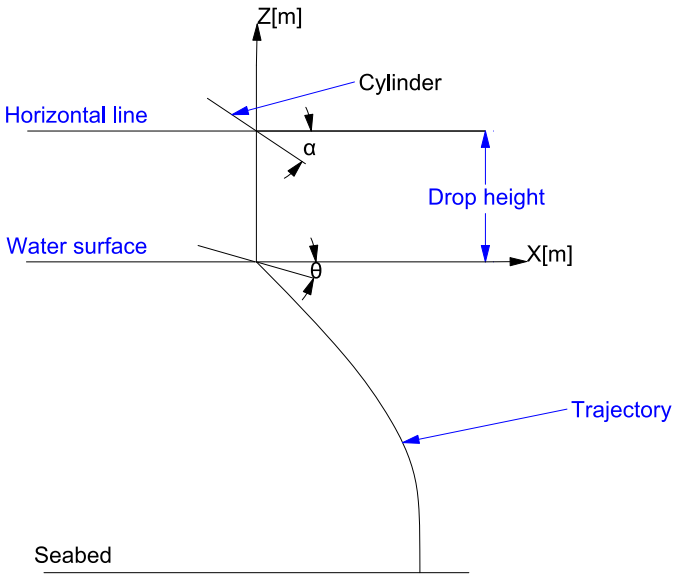

Fig. 2 Set up for model test with dropped cylinders

Cylinder #1 was chosen to compare results with work reported in Chu, Gilles *et al*. (2005). The cylinder is trimmed nose down with a positive longitudinal center of buoyancy LCG=0.0074 m. Additional data are reported in Table 1. The starting point for the cylinder is a fixed position above the water surface and a defined drop angle. The cylinder is then released and freely drops into calm water and sinks until it hits the seabed. For the experiments a water depth of 2.4 m is reported. The principal setup of the cylinder is illustrated in Fig. 2 where α is the drop angle, θ is the instantaneous orientation angle (Euler angle) around the Y-axis, with θ_0 being the initial orientation angle around the Y-axis when the cylinder has fully entered the water.

In Chu et al.'s experiments (2005), the following initial conditions have been determined for the underwater motions

$$
\begin{array}{lll}
X_0 = 0\ \text{m} & Y_0 = 0\ \text{m} & Z_0 = 0\ \text{m} \\
\dot{X}_0 = 0\ \text{m/s} & \dot{Y}_0 = -1.55\ \text{m/s} & \dot{Z}_0 = -2.52\ \text{m/s} \\
\phi_0 = 0^o & \theta_0 = 60^o & \psi_0 = -95^o \\
\Omega_{10} = 0\ \text{rad/s} & \Omega_{20} = 0.49\ \text{rad/s} & \Omega_{30} = 0.29\ \text{rad/s}
\end{array} \tag{41}
$$

Fig. 3 compares the authors' simulated underwater trajectory of the center of gravity of the cylinder with experimental and simulated results from Chu, Gilles *et al*. (2005). In contrast to the simulation by Chu, Gilles *et al*. (2005) the trajectory predicted from DROBS shows an inflection point in the trajectory which is also visible in the experimental results. The point is marked with a light blue square. The trajectory predicted by DROBS also features the motion in X direction during the second segment of trajectory which follows the model test trajectory. This results in a more accurate prediction of the landing point. Landing point results are compared in Table 2. Additional verification results can be found in Xiang, Birk *et al*. (2016b)

Table 2 Comparison of landing points

Landing points	**Experimental results,** Chu, Gilles *et al*. (2005)	**Simulated results,** Chu, Gilles *et al*. (2005)	**Simulated results DROBS**
X (m)	-0.10	0.05	-0.03
Y (m)	-0.25	-0.50	-0.36

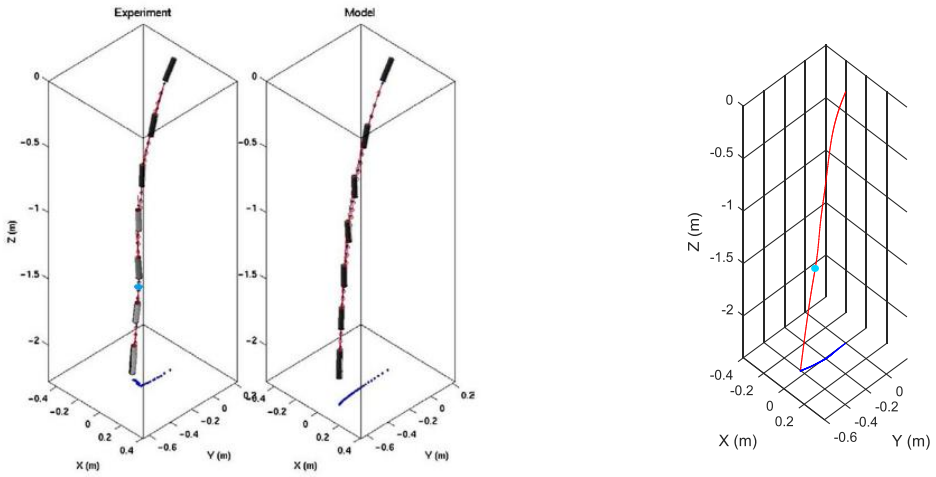

(a) (b)

Fig. 3 Trajectory of cylinder #1 with drop angle 45°: (a) Chu, Gilles *et al*. (2005) and (b) DROBS

3.2 Dropped object: Cylinder #1 under uniform current

In this study, the effects of current on the trajectory is included in the simulation. Effects due to surface waves, however, are ignored. Luo and Davis (1992) found that horizontal excursion at the seabed level is significantly influenced by currents but waves have a limited overall effect. This may be because wave effects will rapidly decay with increasing submergence. We simulate the trajectories of a cylinder with the same properties as cylinder #1. Again the initial conditions as expressed in Eq. (41) are employed. An additional uniform current of 0.5 m/s speed is considered to act across the whole water column. Simulations are conducted for current headings of 0^o, 90^o, 180^o, and 270^o. Fig. 4 presents the resulting trajectories.

The trajectory of the cylinder and its landing point are clearly influenced by currents. Table 3 reports data for simulations of landing points without and with current. For $\beta = 0^o$ (positive X-direction) the landing point shifts in positive X-direction and positive Y-direction by 0.09 m and 0.03 m respectively. The Y-shift being a result of the increased lift force. For the current in negative X-direction ($\beta = 180^o$) the landing point shifts in negative X-direction and negative Y-direction by 0.08 m and 0.04 m. The absolute excursions in X-direction are similar for currents in X-directions ($\beta = 0^o$ and $\beta = 180^o$). However, currents in transverse directions ($\beta = 90^o$ and $\beta = 270^o$) have a significantly larger effect on the total excursion. With current heading at 90^o, the landing point shifts in positive X-direction by 0.01 m and in positive Y direction 0.61 m respectively. With reversed transverse current heading similar values are obtained for movement in negative X- and negative Y-direction. The increased excursions also lead to small increases in drop time for cases with transverse current.

Table 3 Comparison of landing points

Case Number	**1**	**2**	**3**	**4**	**5**
Current Heading	**No current**	$\boldsymbol{\beta = 0^o}$	$\boldsymbol{\beta = 90^o}$	$\boldsymbol{\beta = 180^o}$	$\boldsymbol{\beta = 270^o}$
$V_{current}$ (m/s)	0	0.5	0.5	0.5	0.5
Landing pt. *X* (m)	-0.03	0.06	-0.02	-0.11	-0.06
Landing pt *Y* (m)	-0.36	-0.33	0.25	-0.40	-0.96
Drop time *T(s)*	1.242	1.236	1.246	1.244	1.270
Difference *X*(m)	0.00	0.09	0.01	-0.08	-0.03
Difference *Y*(m)	0.00	0.03	0.61	-0.04	-0.60
Difference T (s)	0.00	-0.006	0.004	0.002	0.028

Notes: Difference X = X(Case N)- X(Case 1), N=1, 2, 3, 4, and 5
Difference Y = Y(Case N)- Y(Case 1), N=1, 2, 3, 4, and 5
Difference T = T(Case N)- T(Case 1), N=1, 2, 3, 4, and 5
T is the duration time until the dropped cylinder lands on the seabed

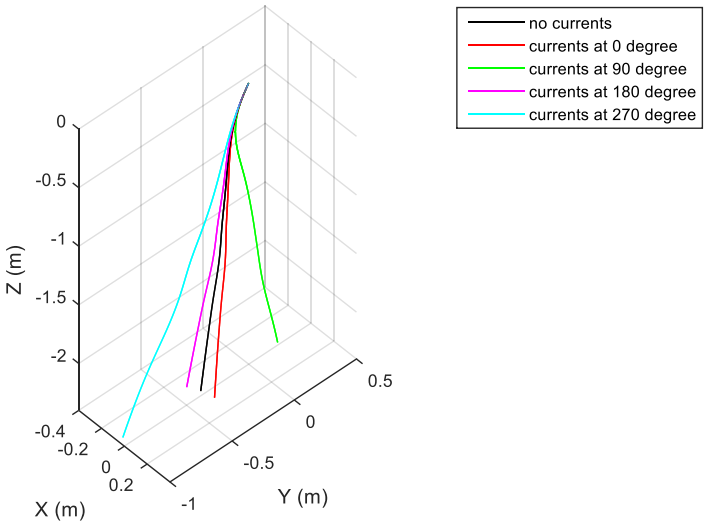

Fig. 4 Trajectory of cylinder #1 under current from direction: β at 0^o, 90^o, 180^o, and 270^o

4. Monte Carlo simulation of landing points

4.1 Monte Carlo simulation

The cylinder used in this set of simulations uses the particulars of the 8" drill pipe model used in Awotahegn (2015). However, here the ends of the pipe are assumed to be closed. Properties of cylinder #2 are listed in Table 4. In Awotahegn's experiments the cylinder was released 1.2 m above the water surface and fell into water of depth 3.0 m. Fig. 5 shows the general setup. The effects of the fall through air may be ignored. However, the impact of the cylinder on the water surface causes unknown changes in drop angle, speed, and rotation. The impact and immersion process are difficult to model and its result depends on many variables. A detailed simulation of the immersion may take too long to support operational decisions on board a vessel. Therefore, the uncertainties in initial conditions are represented with a stochastic model in this paper.

Table 4 Properties of the cylinder #2

Parameters	**Unit**	**Value**
Model Scale		1:16.67
Length	m	0.537
Mass density	kg/m	0.325
Diameter	m	0.013
LCG	m	0.000

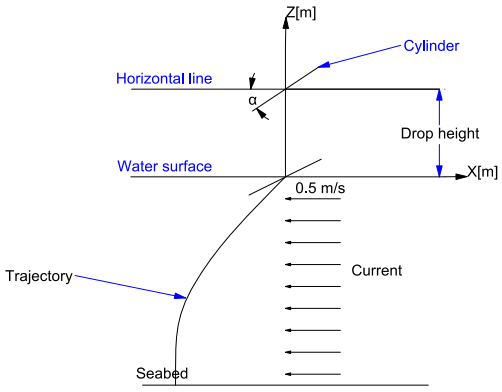

Fig. 5 Schematic setup of dropped cylinder simulation with currents

The Monte Carlo method is just one of many methods for analyzing uncertainty propagation. The goal is to determine how random variations, lack of knowledge, or errors affect the sensitivity, performance, or reliability of the system which is being modeled. Monte Carlo simulation is categorized as a sampling method because the inputs are randomly generated from probability distributions to simulate the process of sampling from an actual population (Dubi 2000).

The uncertainty propagation process shown in Fig. 6, assumes that variables x_1, x_2, and x_3, etc follow a probability density distribution which most closely matches available data, or best represents the current state of knowledge. Since DROBS has been verified to predict landing points of dropped cylinders with reasonable accuracy, DROBS is used as the modeling function *f(x)*. The data (y_1, y_2, etc) generated by the simulation will be the excursion of landing points which may in turn be presented as probability distributions (or histograms), reliability predictions, and confidence intervals.

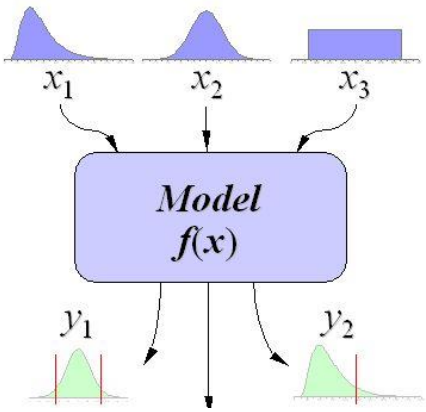

Fig. 6 Schematic showing the principal of stochastic uncertainty propagation (Wittwer 2004)

4.2 Description of random variables

The initial conditions for a drop simulation in DROBS are orientation angles (ϕ_0, θ_0, ψ_0), translational velocities ($\dot{X}_0, \dot{Y}_0, \dot{Z}_0$), and rotational velocities ($\Omega_{10}, \Omega_{20}, \Omega_{30}$) when the cylinder is just fully immersed. Since the equations of motion (1)-(6) are stated in the local coordinate system, the translational velocities given in the global coordinate system ($\dot{X}_0, \dot{Y}_0, \dot{Z}_0$) must first be transformed into the velocities (U_1,U_2, U_3) in the local coordinate system by reversing Eqs. (38)-(40).

With the velocity of center of gravity of cylinder falling in the air is perpendicular to the water surface, during the water entry process, the perturbation of the velocity of the center of gravity is very small in X and Y direction. So the assumption is: $\dot{X}_0 = 0$, $\dot{Y}_0 = 0$, $\phi_0 = 0$. The remaining 6 variables ($\theta_0, \psi_0, \dot{Z}_0, \Omega_{10}, \Omega_{20}, \Omega_{30}$) are called the random variables which are assumed to be independent and follow its own normal distribution, $N(\mu, \sigma^2)$. The out of plane motion variable ($\psi_0, \Omega_{10}, \Omega_{30}$) are assumed to be not significantly influenced by the impact, so the mean value μ is equal to the initial value at the drop point and has a very small deviation σ from mean value μ. This assumption means the variables tend to remain at the initial status with no change or very small change during the water entry process. Variables: Ω_{20} and θ_0, for in plane motion (xz plane) are influenced significantly during the water entry process (Wei 2015), so large standard deviation values are used for σ with 3 for Ω_{20} , 0.6 for θ_0 but the mean value of Ω_{20} and θ_0 also keep the same as their initial value at drop point. Because of energy loss during water entry process, $\dot{Z}_0$ decreases starting from V_{max}. V_{max} is the maximum velocity of dropped cylinder before entering water and estimated by the law of conservation of energy, Eq. (42). But it's hard to estimate how much energy will dissipate during water entry process so the mean value for $\dot{Z}_0$ is tested and set according to 10% velocity loss, 25% velocity loss and 50% velocity loss. The standard deviation σ is set at a very small value: 0.1. The specifications of random variables are shown in Table 5.

$$V_{max} = \sqrt{2gh} \tag{42}$$

Table 5 Specifications of random variables

Random variables	**Units**	**Mean value μ**	**Variance σ^2**
θ_0	rad	α	0.36
ψ_0	rad	0	0.01
		$0.9V_{max}$	0.01
$\dot{Z}_0$	m/s	$0.75V_{max}$	0.01
		$0.5V_{max}$,	0.01
Ω_{10}	rad/s	0	0.01
Ω_{20}	rad/s	0	9.0
Ω_{30}	rad/s	0	0.01

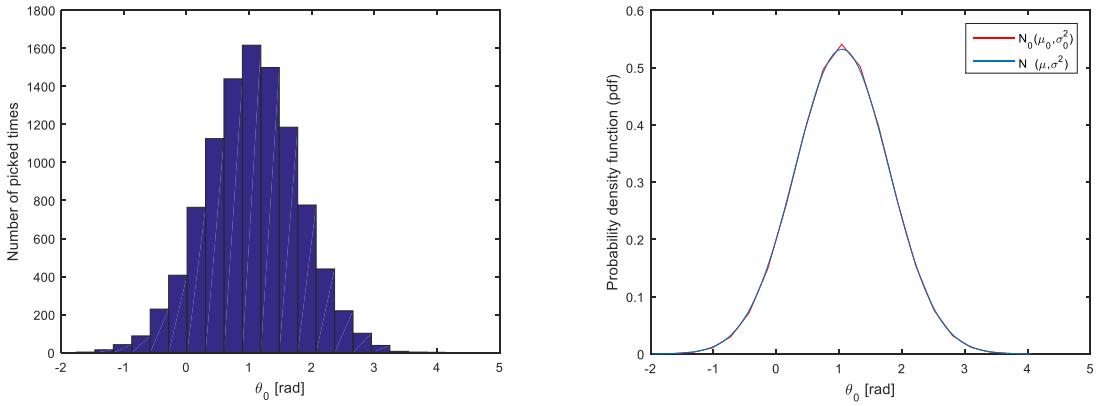

(a) (b)

Fig. 7 Normal distribution of θ_0 : (a) true distribution and (b) sampling distribution

4.3 Sampling process

The sample size used in this Monte Carlo simulation is 10000 which means randomly picking data 10000 times for random variable group $(\theta_0, \psi_0, \dot{Z}_0, \Omega_{10}, \Omega_{20}, \Omega_{30})$. Every random variable is randomly picked from its own normal distribution, $N(\mu, \sigma^2)$. These 10000 samples will form a new sampling distribution, $N_0(\mu, \sigma^2)$. True distribution of θ_0 is $N(1.05, 0.6^2)$ for drop angle 60^o as plotted in Fig. 7(a). The sampling distribution is shown in Fig. 7(b).

4.4 Results of estimated landing point distribution

4.4.1 DNV simplified method

DNV simplified method (DNV, 2010) assumes the landing point on the horizontal position of seabed to be normal distributed with angular deviations defined as Eq. (43)

$$p(X) = \frac{1}{\sqrt{2\pi}\delta} e^{-\frac{1}{2}(\frac{X}{\delta})^2} \tag{43}$$

So the distance between landing point and the vertical line through the drop point will follow

$$p(R) = p(|X|) = \frac{2}{\sqrt{2\pi}\delta} e^{-\frac{1}{2}(\frac{R}{\delta})^2} \tag{44}$$

Where,

X Horizontal position at the seabed (meters)
Y Vertical position at the seabed (meters)
δ Lateral deviation (meters)
R=$\sqrt{X^2+Y^2}$, excursion on the seabed (meters), here, Y=0.
$p(X)$ Probability density of a dropped object landing at position X
$p(R)$ Probability density of a dropped object landing at excursion R

So the probability that a dropped object will land at the seabed within a distance r from the vertical line through the drop point is then expressed by the cumulative distribution function

$$P(R \leq r) = \int_0^r p(R)dR \tag{45}$$

4.4.2 Comparison of landing point distribution under no current and estimation of mean value for $\dot{Z}_0$

As shown in Figs. 8-10, the landing point distribution for Cylinder #2 with drop angle 60° under no current is obtained by multiple Monte Carlo simulations from DROBS. The mean value for $\dot{Z}_0$ is set according to 10% velocity loss, 25% velocity loss and 50% velocity loss after being fully immersed into water. And other variables follow $\psi_0 \sim N(0, 0.1^2)$, $\theta_0 \sim N(\alpha, 0.6^2)$, $\Omega_{10} \sim N(0, 0.1^2)$, $\Omega_{20} \sim N(0, 3^2)$, $\Omega_{30} \sim N(0, 0.1^2)$.

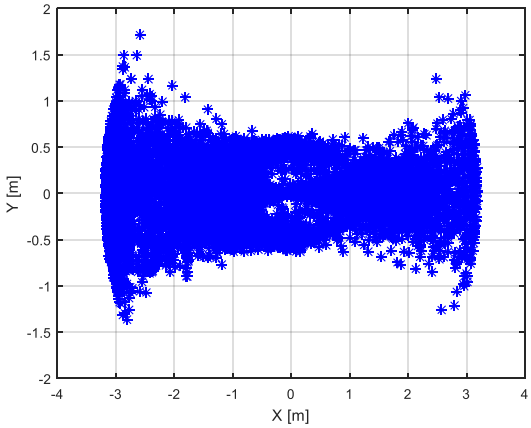

Fig. 8 Landing point distribution drop angle 60° with $\dot{Z}_0 \sim N(0.90V_{max}, 0.1^2)$

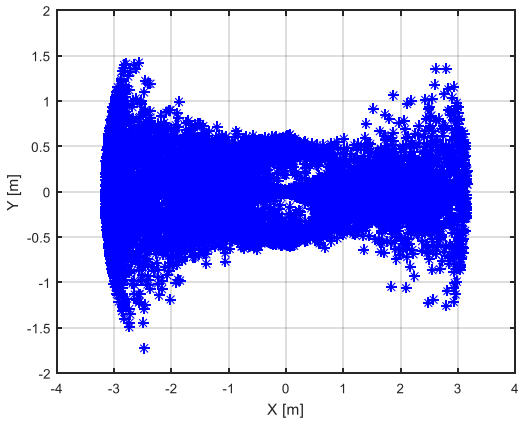

Fig. 9 Landing point distribution drop angle 60° with $\dot{Z}_0 \sim N(0.75V_{max}, 0.1^2)$

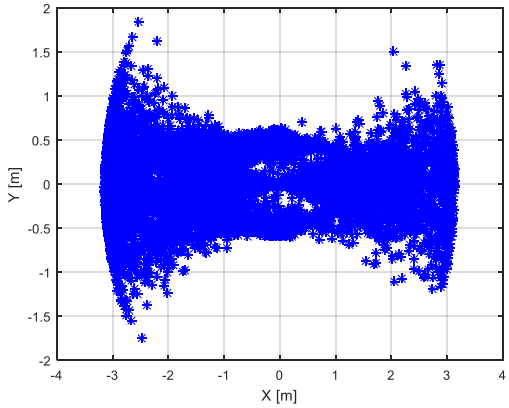

Fig. 10 Landing point distribution drop angle 60° with $\dot{Z}_0 \sim N(0.50V_{max}, 0.1^2)$

Statistical values including mean, median, maximum (Max), minimum (Min), and standard deviation (SD) of excursion of landing points from DROBS based simulated results are compared with experimental results (Awotahegn 2015) as shown in Table 6. It's found that: 1, when the mean value of $\dot{Z}_0$ varies from $0.90V_{max}$ to $0.50V_{max}$, statistical values of excursion of landing points are not sensitive to the change of mean value of $\dot{Z}_0$; 2, the DROBS based Monte Carlo simulation can provide reasonable results though the mean value and standard deviation of simulated results are slightly larger than from experimental results in Awotahegn, (2015). Firstly, this may be because the sample size in experiments (Awotahegn 2015) is very small compared with 10000 samples utilized in Monte Carlo simulations which caused the larger statistical values. Also, dropped cylinder with closed ends used in simulation will make a difference from open ends used in real experiments (Awotahegn 2015) on trajectories. By comparing simulated results and experimental results (Awotahegn 2015) with results from simplified method in DNV (2010) in Table 7, it shows the mean value from this simplified method is so small that results in underestimating the possible excursion of a landing point on the sea bed.

Table 6 Comparison of statistical value at different $\dot{Z}_0$ distribution

	Simulated Results (DROBS)					**Experimental Results (Awotahegn 2015)**			
Distribution	Mean (m)	Median (m)	Max (m)	Min (m)	SD (m)	Mean (m)	Max (m)	Min (m)	SD (m)
$N(0.90V_{max}, 0.1^2)$	1.51	1.32	3.23	0.00	0.91	1.13	2.30	0.40	0.42
$N(0.75V_{max}, 0.1^2)$	1.53	1.35	3.17	0.00	0.92	1.13	2.30	0.40	0.42
$N(0.50V_{max}, 0.1^2)$	1.51	1.32	3.16	0.00	0.91	1.13	2.30	0.40	0.42

Table 7 Landing point distribution from simplified method in DNV (2010)

DNV simplified method	
Mean (m)	SD (m)
0.64	0.80

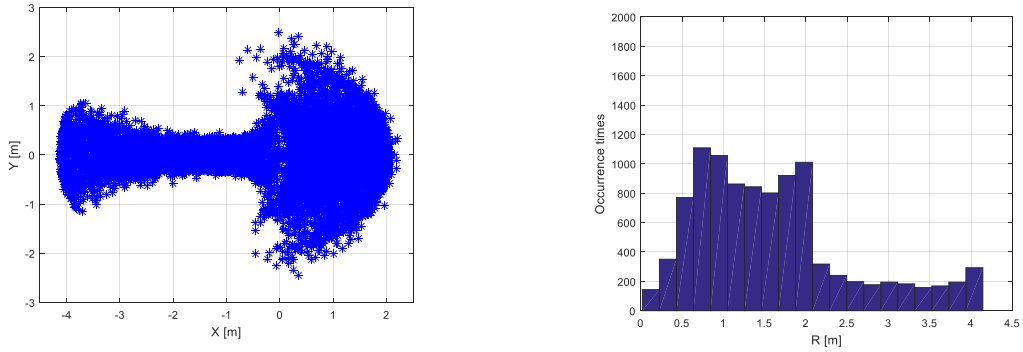

(a) (b)

Fig. 11 Drop angle 0° with $\dot{Z}_0 \sim N(0.5V_{max}, 0.1^2)$, $\theta_0 \sim N(0, 0.6^2)$, $\Omega_{20} \sim N(0, 3^2)$: (a) Landing point distribution and (b) Histogram of excursion

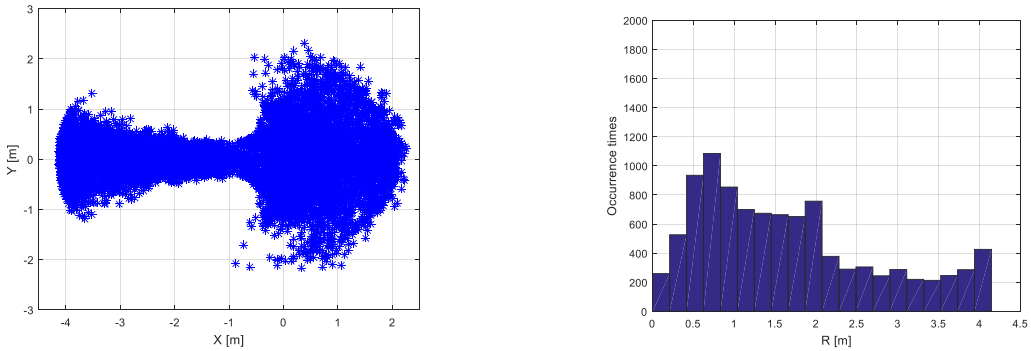

(a) (b)

Fig. 12 Drop angle 15° with $\dot{Z}_0 \sim N(0.5V_{max}, 0.1^2)$, $\theta_0 \sim N(0.26, 0.6^2)$, $\Omega_{20} \sim N(0, 3^2)$: (a) Landing point distribution and (b) Histogram of excursion

4.4.3 Simulated landing point distributions under uniform current

At drop angle 0^o , 15^o , 30^o , 45^o , 60^o , 75^o ,and 90^o , the landing point distribution for Cylinder #2 under uniform current with velocity 0.5 m/s and incoming angle β at 180^o, are obtained from Monte Carlo simulations as shown in Figs. 11(a)-17(a). Also, corresponding histogram of the excursion, R is provided for each drop angle to visualize the uncertainty in landing points distribution.

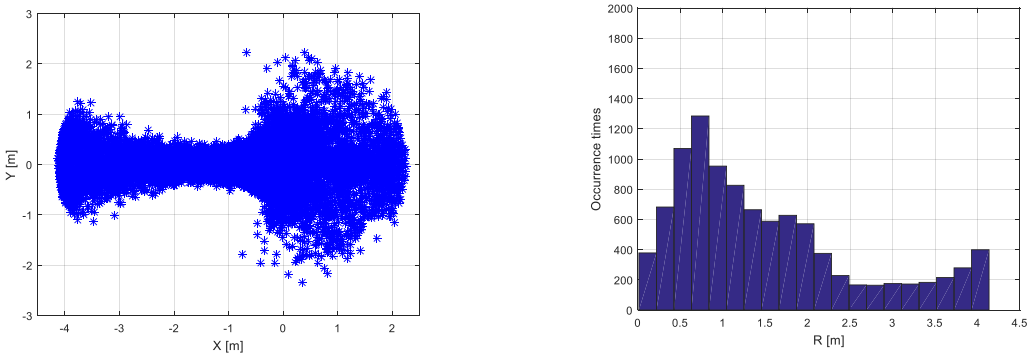

(a) (b)

Fig. 13 Drop angle 30^o with $\dot{Z}_0 \sim N(0.5V_{max}, 0.1^2), \theta_0 \sim N(0.52, 0.6^2), \Omega_{20} \sim N(0, 3^2)$: (a) Landing point distribution and (b) Histogram of excursion

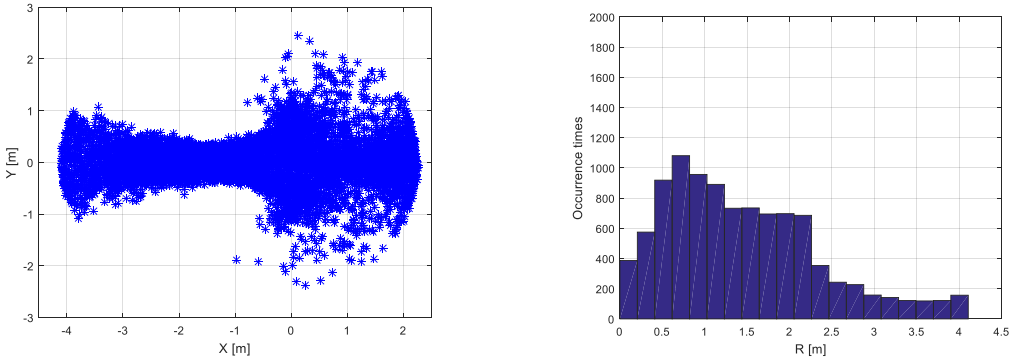

(a) (b)

Fig. 14 Drop angle 45^o with $\dot{Z}_0 \sim N(0.5V_{max}, 0.1^2, \theta_0 \sim N(0.79, 0.6^2), \Omega_{20} \sim N(0, 3^2)$: (a) Landing point distribution and (b) Histogram of excursion

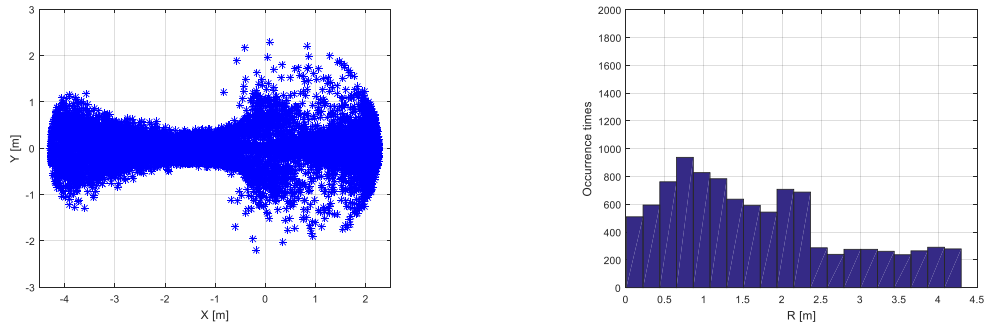

(a) (b)

Fig. 15 Drop angle 60° with $\dot{Z}_0 \sim N(0.5V_{max}, 0.1^2), \theta_0 \sim N(1.05, 0.6^2), \Omega_{20} \sim N(0, 3^2)$: (a) Landing point distribution and (b) Histogram of excursion

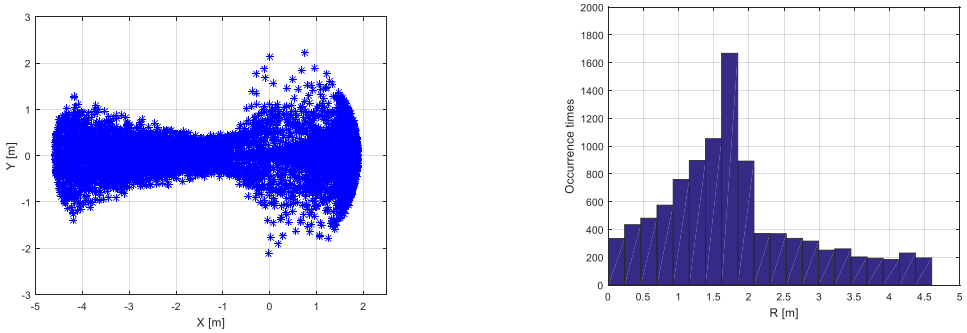

(a) (b)

Fig. 16 Drop angle 75° with $\dot{Z}_0 \sim N(0.5V_{max}, 0.1^2), \theta_0 \sim N(1.31, 0.6^2), \Omega_{20} \sim N(0, 3^2)$: (a) Landing point distribution and (b) Histogram of excursion

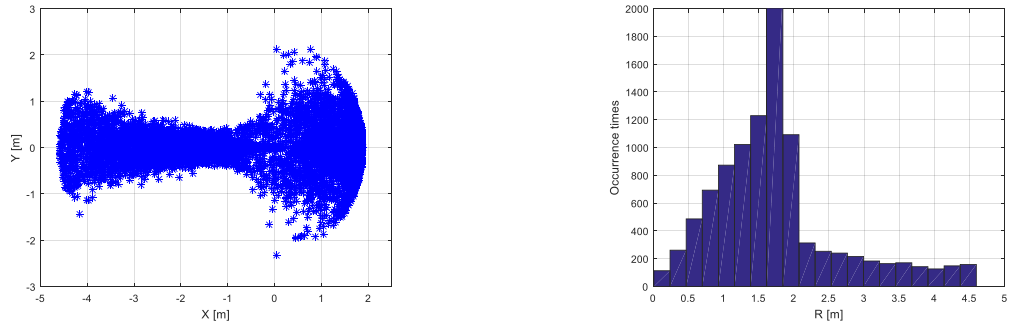

(a) (b)

Fig. 17 Drop angle 90° with $\dot{Z}_0 \sim N(0.5V_{max}, 0.1^2), \theta_0 \sim N(1.57, 0.6^2), \Omega_{20} \sim N(0, 3^2)$: (a) Landing point distribution and (b) Histogram of excursion

Table 8 Comparison of statistical value at different drop angles

Simulated Results					
Drop angle	Max (m)	Min (m)	Mean(m)	SD (m)	89% confidence interval (m)
0^o	4.14	0.02	1.59	0.94	0-4.41
15^o	4.14	0.00	1.66	1.08	0-4.90
30^o	4.13	0.01	1.51	1.07	0-4.72
45^o	4.10	0.00	1.45	0.91	0-4.18
60^o	4.29	0.00	1.70	1.12	0-5.06
75^o	4.60	0.00	1.83	1.04	0-4.95
90^o	4.60	0.01	1.75	0.90	0-4.45

4.5 Statistical analysis of simulated landing point distribution

4.5.1 Mean, Median, Maximum (Max), Minimum (Min), Standard Deviation (SD) and confidence interval of excursion

The statistical values of excursion of landing point are shown in Table. 8

The maximum mean value of excursion happens at drop angle, 75^o. By considering standard deviation and mean value together, 89% confidence interval can be obtained based on Chebyshev's inequality theory (Mood, Graybill *et al.* 1974) in Eq. (46). The maximum 89% confidence interval is between 0-5.06m at drop angle, 60^o.

$$P(|R-\mu|) \geq k\sigma) \leq \frac{1}{k^2}, k > 1 \tag{46}$$

When $k = 3$, $P(|R-\mu|) < 3\sigma) \geq \frac{8}{9} \approx 89\%$. So the 89% confidence interval is between $\mu - 3\sigma$ and $\mu + 3\sigma$.

4.5.2 Risk free zone

By analyzing all the excursion data of landing points for drop angle at $0^o, 15^o, 30^o, 45^o, 60^o, 75^o$ and 90^o, an overall probability distribution of landing points are represented by Probability Density Function (PDF) in Fig. 18 and Cumulative Distribution Function (CDF) in Fig. 19. It's found that in the PDF curve as depicted in Fig. 18, dropped cylinder is most likely to land at excursion: R=1.80 m. Corresponding to R exceeding 1.80 m, its probability drops significantly.

The probability of landing point within a certain *r* is presented as $p(R \leq r)$. As shown in Fig. 19, the cylinder drops within 1m($R \leq 1\ m$) with 30% of probability and within 3.3 m ($R \leq$ 3.3 m) with 90% of probability. Then, the probability of a landing point beyond a certain *r* is described by $p(R > r)$ =1- $p(R \leq r)$. If $p(R > r)$ is small enough, it may be called risk free. Then the risk free zone is the area beyond *r*. The details about risk free zone are shown in Table 9 and Fig. 19.

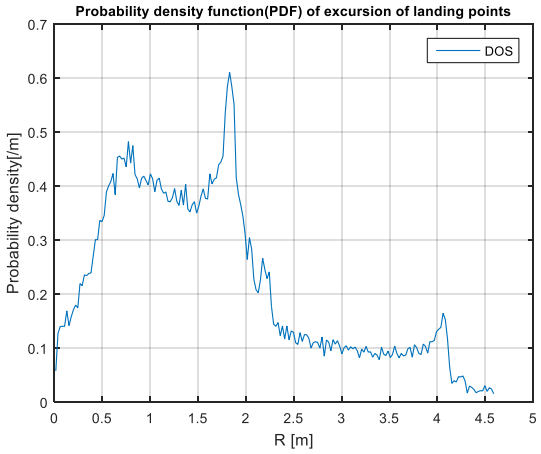

Fig. 18 PDF of excursion of landing points, R with $\dot{Z}_0 \sim N(0.5V_{max}, 0.1^2), \theta_0 \sim N(\alpha, 0.6^2), \Omega_{20} \sim N(0, 3^2)$

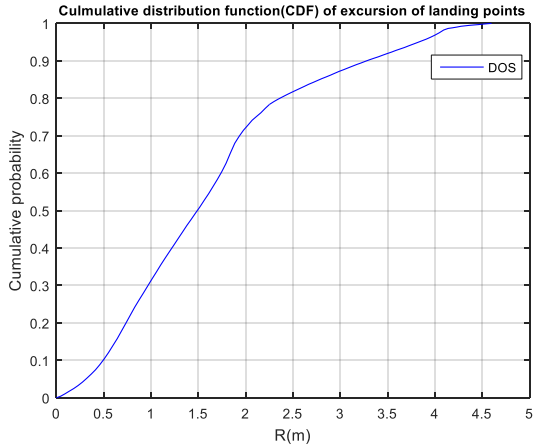

Fig. 19 CDF of excursion of landing points, R with $\dot{Z}_0 \sim N(0.5V_{max}, 0.1^2), \theta_0 \sim N(\alpha, 0.6^2), \Omega_{20} \sim N(0, 3^2)$

Table 9 Details of risk free zone

$p(R > r)$	**risk free zone**
0.10	$R > 3.3\ m$
0.05	$R > 3.8\ m$
0.01	$R > 4.4\ m$

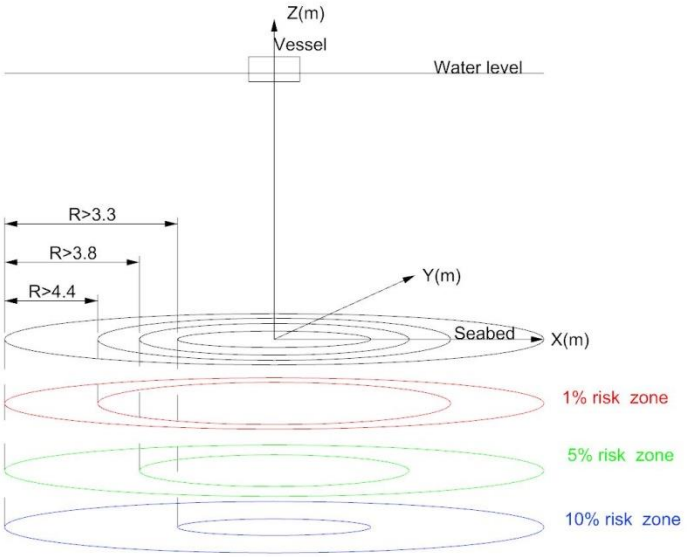

Fig. 20 CDF of excursion of landing points, R with $\dot{Z}_0 \sim N(0.5V_{max}, 0.1^2), \theta_0 \sim N(\alpha, 0.6^2), \Omega_{20} \sim N(0, 3^2)$

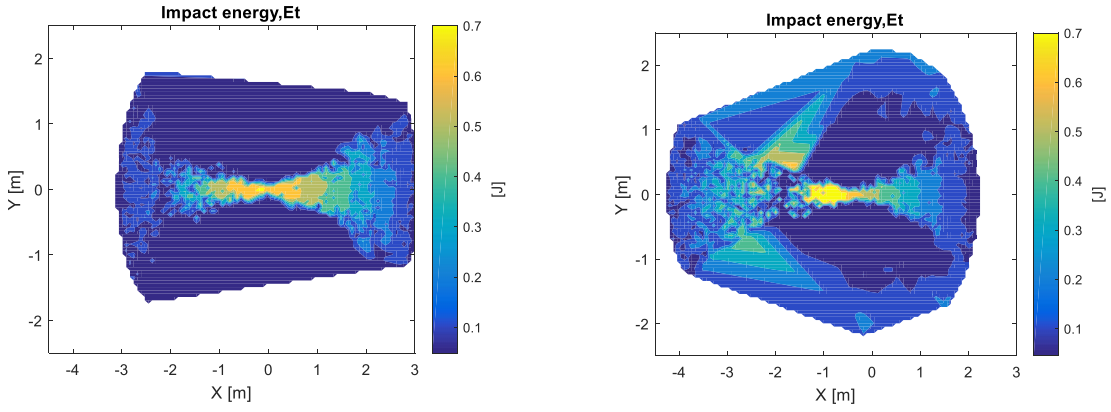

(a) (b)

Fig. 21 impact energy distribution for drop angle at 60°: (a) without current and (b) current with speed 0.5 m/s and incoming angle β at 180^o

Also, impact energy distribution of a dropped object at seabed is another criteria to co-work with Fig. 19 to build up the complete risk assessment. The impact energy is estimated by (DNV, 2010).

$$E_t = \sum_{i=1}^{3} \frac{1}{2}(m + m_{ii})v_{ti}^2 \tag{47}$$

E_t is the total impact energy at the sea bed; m_{ii} is 3D added mass coefficient in the *i*th

direction. v_{ti} is the terminal velocity at the sea bed in the *i*th direction.

Figs. 20(a) and 20(b) represent the impact energy distribution of a dropped object at drop angle, 60^o under no current and under 0.5m/s current respectively. By comparing Figs. 20(a) and 20(b), the high impact energy area marked yellow is greatly influenced by the current and moved in the direction of current and spread out at the downstream of the current.

5. Conclusions

In this paper, the authors developed the 3D theory in Xiang, Birk *et al.* (2016b) to consider the underwater dynamic motion of a dropped cylindrical object under current from different directions. Correspondingly, an updated numerical tool, DROBS is utilized to investigate how uniform current from different directions (incoming angle at 0^o, 90^o, 180^o, and 270^o) affects the trajectories of dropped cylinder. It's found that the trajectories and landing points of the dropped cylinder are greatly influenced by the direction of current. Further, the water entry of the dropped cylinder into calm water are considered as stochastic process which makes the values for orientation angle, translational velocity and rotational velocity of the cylinder after being fully immersed follow normal distributions. Firstly, the Monte Carlo simulations of landing points of dropped cylinder with drop angles at 60^o through air-water columns without current are accomplished in DROBS. It's found that DROBS based Monte Carlo simulations can provide reasonable landing point distribution. Also, the mean value obtained from simplified method in DNV (2010) is too low to describe the landing point distribution of a dropped cylinder. Then, the Monte Carlo simulations are used for predicting the landing point distribution of dropped cylinder under current with drop angle from 0^o to 90^o. It's found that the maximum mean value happens at drop angle, 75^o. Lastly, the overall landing point distribution plots: Probability Density Function (PDF) and Cumulative Distribution Function (CDF) are provided to help study the uncertainty of landing point and also to set the risk-free zone. What's more, the impact energy distribution at seabed for dropped cylinder under current and no current are presented to provide another criteria to do risk assessment of possible damage to subsea equipment.

References

Aanesland, V. (1987), "Numerical and experimental investigation of accidentally falling drilling pipes", *Annual OTC in Houston*, Texas, April 27-30.

American Bureau of Shipping, (2013), *Guidance notes on accidental load analysis and design for offshore structures*, ABS, Houston, TX, USA.

Awotahegn, M.B. (2015), *Experimental investigation of accidental drops of drill pipes and containers*, Master Thesis, University of Stavanger.

Chu, P.C., Gilles, A. and Fan, C.W. (2005), "Experiment of falling cylinder through the water column", *J. Exper. Therm. Fluid Sci*., **29**(5), 555-568.

Chu, P.C. and Fan, C.W. (2006), "Prediction of falling cylinder through air-water-sediment columns", *J. Appl. Mech. Rev. – ASME*, **73**, 300-314.

Colwill, R.D. and Ahilan, R.V. (1992), "Reliability analysis of the behavior of dropped objects", *24th Annual OTC* in Houston, Texas

DNV (1996), *Worldwide offshore accident databank (WOAD)*, version4.11

DNV (2010), *Risk assessment of pipeline protection*, RP-F107

Dropped Objects Register of Incidents & Statistics (DORIS) (2016), http://www.doris.dropsonline.org/

Dubi, A. (2000), *Monte Carlo applications in systems engineering*. Wiley, West Sussex, U.K.

Glenn Research Center (1941), *Kutta-Joukowski lift theorem for a cylinder* https://www.grc.nasa.gov/www/k-12/airplane/cyl.html (accessed 16.03.15)

Hoerner, S.F. (1958), *Fluid dynamics drag*, Bricktown, NJ

John, M.S. and Francis, E.P. (1962), *Six-degree-of-freedom equations of motion for a maneuvering re- entry vehicle*, Technical Report, NAVTRADEVCEN 801A

Luo, Y. and Davis, J. (1992), "Motion simulation and hazard assessment of dropped objects", *Proceedings of the 2nd International Offshore and Polar Engineering Conference*, ISBN 1-880653-04-4 San Francisco, USA.

Mood, A.M., Graybill, F.A. and Boes, D.C. (1974), *Introduction to the theory of statistics*, McGraw- Hill Book Company, New York

Majed, A. and Cooper, P. (2013), "High fidelity sink trajectory nonlinear simulations for dropped subsea objects", *Proceedings of the 23rd International Offshore and Polar Engineering Conference*, AK,USA

Nagle, R.K., Saff, E.B. and Snider, A.D. (2008), *Fundamentals of differential equations and boundary value problems*, 5th Ed., Pearson Education, Inc. Boston, Massachusetts.

Newman, J.N. (1977), *Marine hydrodynamic*, The MIT Press, Cambridge, Massachusetts.

Rouse, H. (1938), *Fluid mechanics for hydraulic engineers*, 1st Ed., McGraw-Hill Book Company, New York.

Schlichting, H. (1979), *Boundary layer theory*, McGraw-Hill Book Company, New York.

Wei, Z.Y. and Hu, C.H. (2015), "Experimental study on water entry of circular cylinders with inclined angles", *J. Mar Sci. Technol*., **20**(4), 722-738.

Wittwer, J.W. (2004), *Monte Carlo simulation Basics*, http://vertex42.com/ExcelArticles/mc/MonteCarloSimulation.html (accessed 16.05.26)

Xiang, G., Birk, L., Yu, X.C. and Lu, H.N. (2016a), "Numerical study on the trajectory of dropped cylindrical objects", Submitted to *J. Ocean Engineering.*

Xiang, G., Birk, L., Yu, X.C. and Li, X. (2016b), "Study on the trajectory and landing points of dropped cylindrical object with different longitudinal center of gravity", Submitted to *J. ISOPE.*

Yasseri, S. (2014), "Experiment of free-falling cylinders in water", *Underwater Technol.*, **32**(2), 177-191.

MK